Interaction-range effects for fermions in one dimension

Martin Hohenadler,[1] Stefan Wessel,[2] Maria Daghofer,[3] and Fakher F. Assaad[1]
[1]*Institut für Theoretische Physik und Astrophysik, Universität Würzburg, 97074 Würzburg, Germany*
[2]*Institut für Theoretische Festkörperphysik, JARA-FIT and JARA-HPC, RWTH Aachen University, 52056 Aachen, Germany*
[3]*Institut für Theoretische Festkörperphysik, IFW Dresden, 01171 Dresden, Germany*
(Received 18 January 2012; published 9 May 2012)

Experiments on quasi-one-dimensional systems such as quantum wires and metallic chains on surfaces suggest the existence of electron-electron interactions of substantial range and hence physics beyond the Hubbard model. We therefore investigate one-dimensional, quarter-filled chains with a Coulomb potential with variable screening length by quantum Monte Carlo methods and exact diagonalization. The Luttinger liquid interaction parameter K_ρ decreases with increasing interaction strength and range. Experimentally observed values close to $1/4$ require strong interactions and/or large screening lengths. As predicted by bosonization, we find a metal-insulator transition at $K_\rho = 1/4$. Upon increasing the screening length, the charge and spin correlation functions reveal the crossover from dominant $2k_\mathrm{F}$ spin correlations to dominant $4k_\mathrm{F}$ charge correlations, and a strong enhancement of the charge velocity. In the metallic phase, the signatures of spin-charge separation in the single-particle spectrum, spinon and holon bands, remain robust even for rather long-ranged interactions. The charge-density-wave state exhibits backfolded shadow bands.

DOI: 10.1103/PhysRevB.85.195115 PACS number(s): 71.10.Pm, 71.10.Fd, 71.10.Hf

I. INTRODUCTION

The Hubbard model has served as a framework to study strongly correlated electrons for almost five decades.[1] Its relative simplicity compared to more realistic models is largely based on approximating the electron-electron Coulomb interaction by an onsite repulsion U between electrons of opposite spin. The resulting Hamiltonian captures many aspects of strong correlations, including the Mott transition at half filling. Detailed knowledge about the model can be obtained by combining the Bethe ansatz with the bosonization technique.[2] However, experiments on quasi-one-dimensional (1D) systems such as quantum wires,[3] carbon nanotubes,[4] or self-organized atom chains[5] fall outside the range of validity of the Hubbard model. This is evinced by the possibility of an insulating, charge-ordered state at quarter filling, substantial $4k_\mathrm{F}$ charge correlations, or by a Luttinger liquid (LL) interaction parameter smaller than $1/2$. Within a quasi-1D description, these features imply electron-electron interactions of finite range.

The case of one dimension is particularly interesting due to the breakdown of Fermi-liquid theory, the importance of collective excitations, and the emergence of spin-charge separation. These phenomena can be understood in the framework of bosonization,[2,6–8] which provides a description in terms of a few nonuniversal parameters valid asymptotically at long wavelengths and low energies. In particular, knowledge of these parameters fully characterizes the correlation functions.

The 1D Hubbard model, describing a screened, onsite interaction, is a Mott insulator for any $U > 0$ at half filling. Away from half filling, umklapp scattering is not allowed and the system remains metallic. The LL interaction parameter takes on values $1/2 \leqslant K_\rho \leqslant 1$, leading to dominant spin-density-wave correlations. A finite interaction range permits Mott or charge-density-wave (CDW) transitions of the Kosterlitz-Thouless type at other commensurate fillings n, for example, at quarter filling in the U-V model with onsite (U) and nearest-neighbor (V) repulsion.[2] In contrast to the Hubbard model, such transitions occur at a finite critical U determined by the condition $K_\rho = n^2$. The effects of extended-range interactions depend on the details. For example, the intuitive picture of long-range interactions driving the system to strong coupling does not always apply: for spinless fermions, the critical interaction for the metal-CDW transition is larger for the $1/r$ potential than for a nearest-neighbor repulsion;[9] for spinfull fermions, a transition seems to be absent for the unscreened potential up to very strong interactions.[10]

The $1/r$ Coulomb potential realized in, e.g., nanotubes and quantum wires, represents the extreme limit of long-range interactions. The logarithmic divergence of its Fourier transform gives rise to remarkable differences, most notably the metallic Wigner crystal (WC) state with quasi-long-range $4k_\mathrm{F}$ charge correlations,[11,12] and the existence of plasmon excitations. Strictly speaking, the divergence only exists for infinite systems and in the absence of screening. Consequently, the above phenomena are absent for any large but finite interaction range, and the bare Coulomb potential can be regarded as a special point in parameter space distinct from the LL liquid fixed point. The $1/r$ potential has been studied analytically[12–21] and numerically.[9,10,22,23]

The typical experimental situation is most likely intermediate between the Hubbard limit and the bare $1/r$ potential. Within bosonization, a finite interaction range only leads to a renormalization of the LL parameters.[2,24] However, in contrast to the Hubbard model, there exist no analytical methods to calculate the LL parameters exactly for nontrivial cases. Besides, the bosonization results rely on a linear band dispersion, and are valid only at low energies and long wavelengths, a limit which is nontrivial to achieve both in experiment and in numerical simulations. On the other hand, exact numerical methods are valid at all energies and distances and permit, e.g., the calculation of spectral weights of excitations. They provide a quantitative connection to microscopic model parameters and can be used to study intermediate interaction ranges. The 1D nature of the problem makes numerical methods particularly powerful.

In this work, we study the effect of the electron-electron interaction range using exact, large-scale quantum Monte Carlo (QMC) simulations and exact diagonalization. The model chosen here makes significant simplifications over typical experimental situations, but we believe that our findings are rather general. One of the key results is the LL interaction parameter K_ρ, which allows us to estimate the interaction strength and range required to reproduce the experimentally observed values. We also study the evolution of static and dynamical correlation functions as a function of the interaction range. Importantly, we find that spin-charge separation in the single-particle spectrum is robust against increasing the interaction range. Our work extends previous investigations of spinfull and spinless lattice models,[9,14,21,22,25,26] and continuum simulations.[27–29]

The paper is organized in the following way. In Sec. II, we introduce the model and discuss related previous work. Section III gives details of the numerical methods. Our results are discussed in Sec. IV. Section V contains the conclusions. The Appendix provides details about the application of the continuous-time (CT) QMC method.

II. MODEL

We consider a 1D chain of length L with Hamiltonian

$$\hat{H} = \sum_k \epsilon(k)\hat{n}_k + \sum_{r=0}^{L/2-1} V(r) \sum_{i=1}^{L} \hat{n}_i \hat{n}_{i+r}. \qquad (1)$$

The kinetic term contains the usual 1D tight-binding band structure $\epsilon(k) = -2t\cos k$. The electron density operator (summed over spin σ) at wave vector k (Wannier site i) is given by $\hat{n}_k$ ($\hat{n}_i$), with $\hat{n}_{i\sigma} = c^\dagger_{i\sigma} c_{i\sigma}$. We have set the lattice constant, $\hbar$, and k_B equal to one, and take t as the unit of energy.

The interaction matrix element $V(r)$ is defined as

$$V(r) = \begin{cases} V, & r = 0 \\ V e^{-r/\xi}/2r\,, & r > 0. \end{cases} \qquad (2)$$

The screening length ξ permits us to interpolate between the Hubbard model ($\xi = 0$, $U = 2V$) and long-range Coulomb interaction [$\xi = \infty$, $V(r) \sim 1/r$]. The choice (2) appears more natural than gradually adding more and more matrix elements for increasing distances. The condition $r < L/2$ is due to the use of periodic boundary conditions. $V(r)$ as defined by Eq. (2) satisfies $V(r) \to 0$ as $r \to \infty$ as well as the convexity condition $V(r+1) + V(r-1) \geqslant 2V(r)$ for $r > 1$. In the classical limit (no hopping), this guarantees a $4k_F$ CDW ground state.[14] If the second condition is not met, the competition between $2k_F$ and $4k_F$ charge order can lead to enhanced metallic behavior or even a CDW-metal transition with increasing interaction range, as observed in quarter-filled extended Hubbard models.[25,30] As we show below, our choice of $V(r)$ excludes such phenomena. We have also compared the choice of potential (2) to an Ewald summation for the case of Fig. 10, where the cutoff is expected to be most relevant, but found only minor changes in the form of energy shifts.

The bosonization picture for the model (1), taking into account the lattice, is as follows. At half filling, any $V > 0$ produces a Mott insulator. For commensurate densities n away from half filling and an interaction range greater than or equal to the average particle spacing $1/n$, strong enough interactions cause a CDW transition at the critical point $K_\rho = n^2$, beyond which umklapp scattering becomes a relevant perturbation.[2] The CDW state is characterized by long-range $4k_F$ charge order. In the LL phase, the dominant correlations are $2k_F$ spin-density fluctuations for $K_\rho > 1/3$, and $4k_F$ charge correlations for $K_\rho < 1/3$. For the unscreened Coulomb potential with divergent Fourier transform ($\xi = \infty$), we formally have $K_\rho = 0$, which would suggest an insulating ground state, in contrast to the continuum prediction of a metallic quasi-WC made by Schulz.[12]

The existence of a metal-insulator transition at $K_\rho = n^2$ has been verified numerically for the U-V model and the U-V_1-V_2 model. In contrast, for lattice fermions with a long-range potential (more specifically, the Pariser-Parr-Pople model), numerical results[10] suggest a metallic ground state with the properties predicted in the absence of umklapp scattering.[12] This rather surprising result, obtained on large but finite systems, is attributed to the reduction of the umklapp matrix element g_3 due to long-range interactions.[9] Within bosonization, there are subtle but important differences between spinfull and spinless models (concerning umklapp scattering), and between odd and even filling factors (e.g., $n = 1/2$ and $1/3$ are not equivalent when considering the Luther-Emery point).[2] These differences seem to manifest themselves also in numerical studies of lattice models. For example, whereas spinfull fermions interacting via a $1/r$ potential remain metallic even for large V,[10] a metal-insulator transition has been observed in the spinless case,[25] with the critical interaction being larger than for the extended Hubbard model.

For simplicity, we consider in the following only the case $\xi < \infty$, so that no divergence in the Fourier transform $V(q)$ occurs. We further focus on quarter filling $n = 0.5$, and will see below that the model (1) is then either a LL (for $K_\rho > 1/4$) or a CDW insulator (for $K_\rho < 1/4$).

For quarter filling, $n = 0.5$, most of the physics of the model (1) (with $\xi < \infty$) can also be captured by simpler U-V or U-V_1-V_2 models provided the convexity condition is satisfied.[14] In particular, these models realize the non-Hubbard regime $K_\rho < 1/2$, and a metal-insulator transition at $K = 1/4$. In the metallic phase, the LL conjecture implies that given the same LL parameters, the extended Hubbard models and Eq. (1) produce identical results, albeit with different microscopic parameters. However, in connection with experiments, it is crucial to know how strong the dependence of the LL parameters and hence the static and dynamical correlation functions on the interaction range is. We will show below that in order to reach the same value of K_ρ, the U-V model requires much larger (and thus rather unrealistic) interactions than a model with a larger interaction range.

III. METHODS AND OBSERVABLES

The majority of our results were obtained from simulations in the stochastic series expansion (SSE) representation with directed loop updates.[31,32] The inclusion of the long-range interaction terms in Eq. (2) is straightforward. Due to the linear scaling of computing time with the average expansion

order, this method permits us to study low temperatures and long chains (up to $L = 140$ here) even in the strong-coupling regime. We also show results obtained with the continuous-time QMC method.[33,34] The latter is restricted to weak and intermediate interactions due to a less favorable scaling of computer time with temperature and system size, and additional numerical difficulties (see the Appendix). Both QMC methods are exact.

The single-particle spectral function is of particular interest in relation to photoemission results. Since the calculation of the single-particle Green's function in SSE is hampered by a minus-sign problem (for periodic boundaries), we instead present results from exact diagonalization on clusters with $L = 20$.

We consider the static charge (ρ) and spin (σ) structure factors

$$S_\rho(q) = \sum_r e^{iqr} \left(\langle \hat{n}_r \hat{n}_0 \rangle - \langle n_r \rangle \langle n_0 \rangle\right),$$
$$S_\sigma(q) = \sum_r e^{iqr} \langle \hat{S}^z_r \hat{S}^z_0 \rangle, \tag{3}$$

where $\hat{S}^z_j = \frac{1}{2}(\hat{n}_{j\uparrow} - \hat{n}_{j\downarrow})$, and the dynamical charge and spin structure factors

$$S_\rho(q,\omega) = \frac{1}{Z} \sum_{ij} e^{-\beta E_j} |\langle i| \hat{\rho}_q |j\rangle|^2 \delta(E_i - E_j - \omega), \tag{4}$$

$$S_\sigma(q,\omega) = \frac{1}{Z} \sum_{ij} e^{-\beta E_j} \left|\langle i| \hat{S}^z_q |j\rangle\right|^2 \delta(E_i - E_j - \omega), \tag{5}$$

where $\hat{\rho}_q = \sum_r e^{iqr}(\hat{n}_r - n)/\sqrt{L}$, and $|i\rangle$ and $|j\rangle$ are eigenstates with energies E_i and E_j. These dynamical correlation functions can be calculated in the SSE representation at fixed particle density and for periodic boundaries without a sign problem. For the analytical continuation, we have used the maximum entropy method.[35]

The $T = 0$ single-particle spectral function reads as

$$A(k,\omega) = A^+(k,\omega) + A^-(k,\omega),$$
$$A^+(k,\omega) = \sum_n \left|\langle \psi^{(N_e+1)}_{n,k} | c^\dagger_{k-q} | \psi^{(N_e)}_{0,q} \rangle\right|^2 \times \delta\left[\omega - \left(E^{(N_e+1)}_{n,k} - E^{(N_e)}_{0,q}\right)\right],$$
$$A^-(k,\omega) = \sum_n \left|\langle \psi^{(N_e-1)}_{n,k} | c_{k-q} | \psi^{(N_e)}_{0,q} \rangle\right|^2 \times \delta\left[\omega + \left(E^{(N_e-1)}_{n,k} - E^{(N_e)}_{0,q}\right)\right], \tag{6}$$

where A^- (A^+) is related to photoemission (inverse photoemission), and $|\psi^{(N_e)}_{0,k}\rangle$ denotes the ground state for the sector with N_e electrons and total momentum k; the corresponding energy is $E^{(N_e)}_{0,k}$. In order to measure energies relative to the Fermi energy, we show $A(k,\omega-\mu)$ with $\mu = [E^{(N_e+1)}_0 - E^{(N_e-1)}_0]/2$.

IV. RESULTS

Since we used three different methods, let us state here that the results of Figs. 1–5, 7, and 8 were obtained using the SSE representation, Fig. 6 with the CTQMC method, and Figs. 9–11 by exact diagonalization. Except for Fig. 2(b), results are for quarter filling $n = 0.5$.

A. Luttinger liquid interaction parameter

In the metallic regime of the model (1), the knowledge of the LL interaction parameter K_ρ together with the bosonization results for the correlation functions provides a complete description of the low-energy, long-wavelength physics. The crossover between the Hubbard and long-range cases as a function of ξ, and the quantitative relation between microscopic parameters and LL parameters, can be studied exactly by means of numerical methods. The LL parameter has previously been calculated, for example, for spinless fermions with a $1/r$ potential,[9] for the U-V model,[36] and for the U-V_1-V_2 model.[30]

We extract K_ρ from SSE QMC results for the charge structure factor using the relation

$$K_\rho = \lim_{L\to\infty} \frac{\pi}{q_1} S_\rho(q_1), \tag{7}$$

where $q_1 = 2\pi/L$ is the smallest, nonzero wave vector for a given system size, and the static structure factor is defined in Eq. (3). For each V and ξ, we have performed a finite-size scaling to obtain K_ρ. The extrapolation is shown for selected values of ξ in the case $V/t = 3$, $n = 0.5$ in Fig. 1. We find that for large enough system sizes, the finite-size dependence is dominated by the lowest order $1/L$, and have therefore used a linear fit for the extrapolation.

Figure 2(a) shows the dependence of K_ρ on V/t and ξ at quarter filling $n = 0.5$. The $V/t = 1$ results fall into the Hubbard regime $K_\rho \geqslant 1/2$ for all values of ξ shown. For a stronger interaction $V/t = 3$, K_ρ becomes smaller than $1/2$ for $\xi \approx 2$, but remains larger than $1/3$, thereby implying dominant $2k_F$ correlations [see Eq. (8) and discussion below]. At $V/t = 6$, the values of K_ρ span the Hubbard, non-Hubbard, and dominant $4k_F$ (i.e., $K_\rho < 1/3$) regimes. For the largest

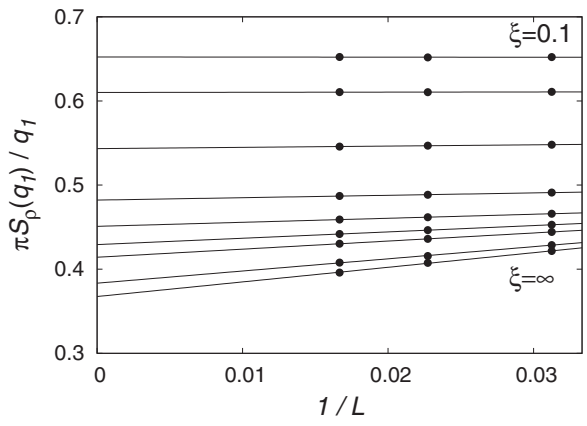

FIG. 1. Finite-size scaling of the rescaled density structure factor $\pi S_\rho(q_1)/q_1$, with $q_1 = 2\pi/L$, for $V/t = 3$, $n = 0.5$, and $\xi = 0.1$, 0.5, 1, 2, 3, 4, 5, 10, 20 (top to bottom). Lines are linear fits, and the extrapolated value in the thermodynamic limit $L \to \infty$ defines the Luttinger liquid parameter K_ρ. The extrapolation has been carried out for all data points shown in Fig. 2. The system sizes were $L = 32,44,60$ for $n = 0.5$ and $L = 60,100,140$ for $n = 0.1$. The temperature was $\beta t = 2L$ for $V/t = 1$ and $\beta t = L$ for $V/t = 3,6,9$.

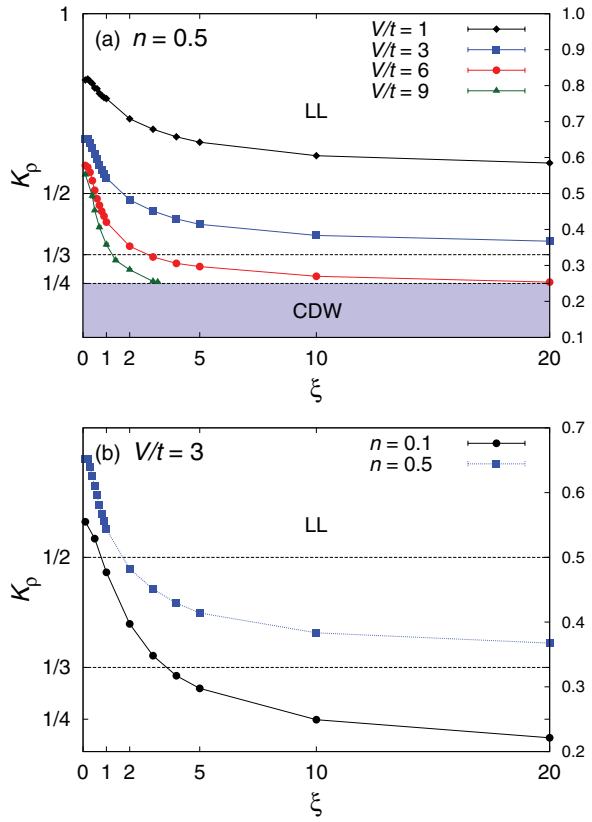

FIG. 2. (Color online) Luttinger liquid parameter K_ρ as a function of screening length ξ. Points represent values obtained from a finite-size scaling (see Fig. 1). Lines are guides to the eye. (a) Results at quarter filling $n = 0.5$. (b) Fixed $V/t = 3$ and different fillings n. The phases are a Luttinger liquid (LL) for $K_\rho > n^2$ and a charge-density-wave insulator (CDW) for $K_\rho < n^2$.

$\xi = 20$, the LL parameter takes on almost exactly the critical value $K_\rho = 1/4$ of the LL-CDW transition. The numerical results therefore suggest that the experimentally observed values of $K_\rho \approx 0.25$ require surprisingly large values of V/t and ξ. Finally, for $V/t = 9$, the system undergoes the metal-insulator transition for $\xi \approx 3.5$. Independent of V, we expect $K_\rho \to 0$ for $\xi \to \infty$ in the thermodynamic limit, corresponding to the quasi-WC. A theoretical prediction $K_\rho \sim \ln^{-1/2} \xi$ was made by Schulz,[12] and the numerical results for the charge structure factor by Fano *et al.*[10] are consistent with $K_\rho = 0$.

Figure 2(a) reveals that K_ρ decreases with increasing ξ, thereby bringing the system closer to the insulating phase. In previous work on extended Hubbard models, it was found that adding interactions at distances beyond the interparticle spacing $1/n$ can increase K_ρ and hence enhance the metallic character of the system.[9,25] Similarly, in the U-V_1-V_2 model with U fixed, varying the relative strength of V_1 and V_2 leads to a competition between $2k_F$ and $4k_F$ charge fluctuations.[25,30] As a result, K_ρ takes on a maximum for $V_2 = V_1/2$, where the metallic state is most stable, and it is not clear if the U-V_1-V_2 becomes insulating at finite values of V_1 and V_2.[26,30] The condition $V(2) = V(1)/2$ is also realized for the unscreened Coulomb potential, and numerical results suggest that the system remains metallic up to very strong interactions even in the presence of a lattice.[10,25] The experimentally motivated form (2), fulfilling the monotonicity and the convexity condition,[14] favors a $4k_F$ CDW state in the limit $V/t \to \infty$.[14] Similar to previous results for spinless fermions with a $1/r$ potential,[9] K_ρ in Fig. 2 decreases with increasing V/t.

A common feature of the curves in Fig. 2(a) is a pronounced decrease at small values of ξ, followed by a much slower decrease for larger ξ. The numerical results indicate that the change in behavior occurs when the interaction range ξ equals the average particle spacing $1/n = 2$. To verify this hypothesis, we compare in Fig. 2(b) the ξ dependence of K_ρ for two different densities $n = 0.5$ and 0.1 at $V/t = 3$. The curve for $n = 0.1$ indeed exhibits a significant ξ dependence up to much larger ξ. The results for $n = 0.1$ further reveal that for a given V/t, a smaller density requires a significantly larger interaction strength and/or range to reach the critical $K_\rho = n^2$ for the metal-insulator transition (see also Ref. 21).

B. Charge and spin correlation functions

For a model with SU(2) spin symmetry such as Hamiltonian (1), bosonization predicts the decay of charge and spin correlation functions to be determined solely by the parameter K_ρ (since $K_\sigma = 1$) (Ref. 37):

$$\langle n_x n_0 \rangle = -\frac{K_\rho}{(\pi x)^2} + \frac{A_1}{x^{1+K_\rho}} \cos(2k_F x) + \frac{A_2}{x^{4K_\rho}} \cos(4k_F x),$$
$$\langle \hat{S}^z_x \hat{S}^z_0 \rangle = -\frac{1}{(2\pi x)^2} + \frac{B_1}{x^{1+K_\rho}} \cos(2k_F x)\,. \quad (8)$$

The $1/x^2$ dependence of the leading term in both channels is familiar from Fermi-liquid theory. The $2k_F$ and $4k_F$ charge correlations decay to leading order as x^{-1-K_ρ} and x^{-4K_ρ}, respectively. For the Hubbard model, $K_\rho \geqslant 1/2$ and $2k_F$ correlations dominate; taking into account logarithmic corrections not included in Eq. (8), the dominant correlations in this regime are $2k_F$ spin correlations.[2] For models with a nonzero interaction range, the $4k_F$ density oscillations can become dominant for $K_\rho < 1/3$. For the Hubbard model, subdominant $4k_F$ oscillations have been observed in systems with open boundary conditions.[38]

In the opposite limit of a $1/r$ Coulomb potential ($\xi = \infty$) with divergent Fourier transform $V(q) \sim \ln(1/q)$, Schulz[12] obtained

$$\langle \hat{n}_x \hat{n}_0 \rangle = \frac{C_1}{x} e^{-c_2\sqrt{\ln x}} \cos(2k_F x) + C_2 e^{-4c_2\sqrt{\ln x}} \cos(4k_F x),$$
$$\langle \hat{S}^z_x \hat{S}^z_0 \rangle = \frac{D_1}{x} e^{-c_2\sqrt{\ln x}} \cos(2k_F x). \quad (9)$$

Apart from the absence of the $1/x^2$ Fermi-liquid contribution, the most notable difference is that charge correlations are dominated by an unusually slow decay of the $4k_F$ component (slower than any power law). These quasi-long-range $4k_F$ charge oscillations led to the notion of a fluctuating WC, where the wavelength $\lambda = 2\pi/4k_F = 1/n$ is the average distance between fermions. In contrast, the spin sector retains a power-law decay. These continuum results are consistent with numerical work.[10,27]

As emphasized before, the WC results (9) rely on the divergence of the Fourier transform of the potential $V(r)$.

Such a divergence only occurs in the thermodynamic limit, and for $\xi = \infty$. If either of these conditions is not met, the LL forms (8) can be recovered in the long-wavelength limit. Here, we only consider large but finite values of ξ, for which a metal-insulator transition occurs at $K_\rho = n^2 = 1/4$. The CDW state exhibits long-range $4k_F$ charge order. The closest analog of the metallic quasi-WC state in our case is therefore the metallic regime $1/3 > K_\rho > 1/4$ with dominant (power-law) $4k_F$ correlations. As shown in Fig. 2, $K_\rho < 1/3$ is realized for $V/t = 6$ and large ξ, and we explore the similarities to the WC in the following.

Figure 3 shows the charge and spin structure factors as defined in Eq. (3). At $V/t = 3$ and with increasing ξ, we see a slight increase of the $4k_F = \pi$ charge correlations [see Fig. 3(a)]. This effect becomes more noticeable for a stronger repulsion $V/t = 6$, as shown in Fig. 3(b). The inherent length scale $1/n$ again appears in Fig. 3, with the results saturating on the scale of the plots for $\xi \gtrsim 2$. The spin structure factor [Figs. 3(c) and 3(d)] reveals an enhancement of $2k_F = \pi/2$ antiferromagnetic correlations with increasing ξ, which according to Eq. (8) can be related to the reduction of K_ρ. This enhancement is again more pronounced for $V/t = 6$ than for $V/t = 3$.

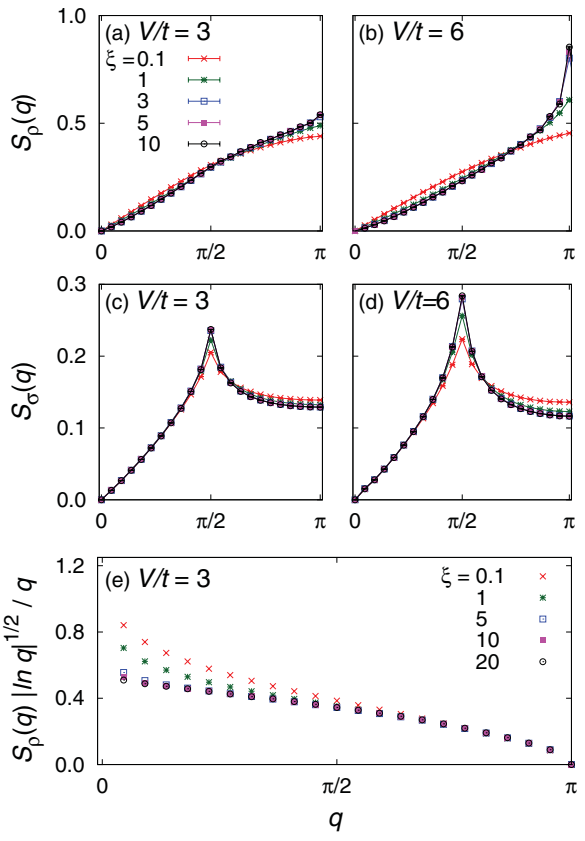

FIG. 3. (Color online) Charge [(a), (b)] and spin [(c), (d)] structure factors $S_{\rho/\sigma}(q)$ for different values of the screening length ξ, and $\beta t = L = 44$. The key in (a) applies to (a)–(d). (e) Rescaled charge structure factor for $V/t = 3$ ($\beta t = L = 60$), revealing the asymptotic approach to the small-q behavior of the WC, $S_\rho(q) \sim q/|\ln q|^{1/2}$. Here and in all subsequent figures, results are for quarter filling $n = 0.5$.

Let us now turn to the long-wavelength behavior. For a LL, we have $S_\rho(q) \sim qK_\rho$, whereas for the WC, $S_\rho(q) \sim q|\ln q|^{-1/2}$ (see Ref. 2). Following Ref. 10, we plot in Fig. 3(e) $S_\rho(q)|\ln q|^{1/2}/q$. This quantity shows a logarithmic divergence at $q = 0$ as long as $S_\rho(q) \sim q$ and tends to a constant as $q \to 0$ for $\xi = \infty$.[10] Our numerical results show that a divergence occurs throughout the metallic phase, and that the approach to the WC result is rather slow. In particular, given the finite values of ξ, the LL nature of the system reemerges eventually in the limit $q \to 0$, although the system sizes required to see this effect become larger and larger. A nonlinear (at long wavelengths) density structure factor corresponding to $K_\rho = 0$ has been observed for the $1/r$ potential.[10] In contrast, for finite ξ, Fig. 3 shows that the linear behavior of $S_\rho(q)$ is preserved. The long-wavelength spin structure factor is not affected by the interactions [Figs. 3(c) and 3(d)]; the slope in the limit $q \to 0$ remains fixed, as required by $K_\sigma = 1$ [cf. Eq. (8)].

Schulz[12] suggested that for a finite ξ, one should be able to observe WC-like correlations at distances $x < \xi$ and LL-like correlations at $x > \xi$. Although the bosonization results are only valid for large distances, this prediction can in principle be tested numerically. Figure 4 shows the density-density correlation function in real space. We have chosen $V/t = 5$, and $\xi = 10$ or 20. This choice was made for the following reasons. First, deviations from the LL form given by Eq. (8) are most visible in the regime where $4k_F$ oscillations dominate, that is, for $K_\rho < 1/3$. However, for the bosonization results to apply, it is important to avoid the insulating state expected for $K_\rho < 1/4$. Close to $K_\rho = 1/4$, previous work on the extended (U-V) Hubbard model has shown the importance of logarithmic corrections.[39] For the parameters chosen, we have $K_\rho \approx 0.29$ for $\xi = 10$ and $K_\rho \approx 0.28$ for $\xi = 20$. The results

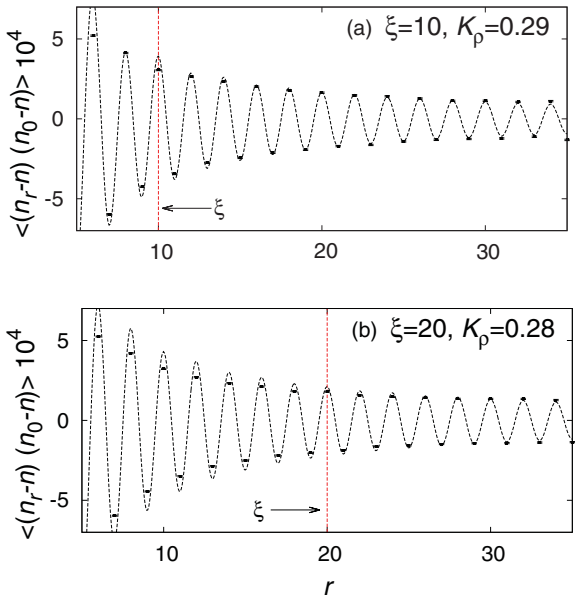

FIG. 4. (Color online) Density-density correlations in real space (symbols). Here, $V/t = 5$, $\beta t = L = 84$, $n = 0.5$ and (a) $\xi = 10$, (b) $\xi = 20$. Lines are fits to the LL result for $\langle n_x n_0 \rangle$ with fitting parameters A_1, A_2 [see Eq. (9)] and K_ρ determined from a (linear) finite-size extrapolation based on $L = 44,84$. The fitting interval was (a) [15 : 35], (b) [25 : 45].

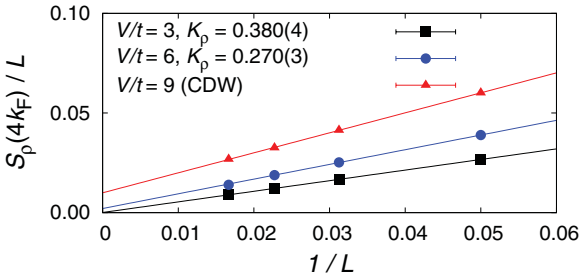

FIG. 5. (Color online) Finite-size scaling of the amplitude of $4k_F$ charge correlations at fixed $\xi = 10$. The results reveal the absence of long-range order for $V/t = 3$, and long-range $4k_F$ charge correlations for $V/t = 9$. The case $V/t = 6$ is on the metallic side but very close to the critical point, and we find a small but finite extrapolated value. The lines are linear fits. Here, $\beta t = L$ and $n = 0.5$.

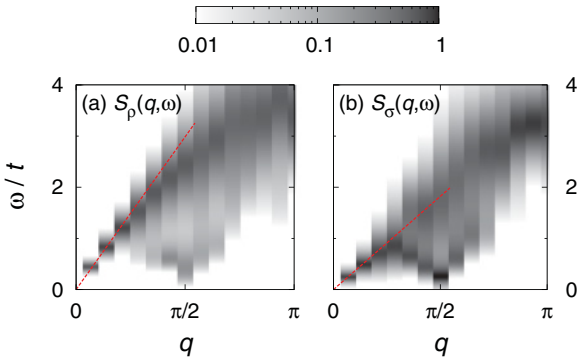

FIG. 6. (Color online) (a) Dynamical charge and (b) spin structure factor for $V/t = 1$ and $\xi = 10$. Results were obtained with the projective CTQMC method (Ref. 34) using $L = 28$, $\theta t = 15$, and $n = 0.5$. Dashed lines indicate the velocity of long-wavelength charge and spin excitations.

in Fig. 4 show dominant $4k_F$ correlations but no long-range order, as expected in the LL regime.

Based on the idea that the LL form for $\langle n_x n_0 \rangle$ should hold at distances larger than ξ, we fit the numerical data to Eq. (8) using two fitting parameters (the $2k_F$ and $4k_F$ amplitudes) as well as the above values of K_ρ. The fitting intervals are chosen as $[\xi + 5, 35]$ and we used $\beta t = L = 84$. Figure 4(a) shows that we indeed have good agreement between the fit and the QMC data at large distances. However, for $r \lesssim \xi = 10$, significant deviations become visible. To discriminate between short-distance effects coming from the continuum approximation underlying Eq. (8) and genuine deviations from LL theory, we consider $\xi = 20$ in Fig. 4(b). Again, there is reasonable agreement at large distances, but clear differences at $r \lesssim \xi = 20$. Hence, keeping in mind the difficulties mentioned above, our results are consistent with the picture proposed by Schulz.[12]

As can be seen from Fig. 2, the insulating CDW phase can be reached for $\xi \gtrsim 3.5$ and $V/t = 9$. The CDW state is characterized by long-range $4k_F$ charge order at $T = 0$, as formally reflected by Eq. (8) for $K_\rho = 0$, and may be regarded as a WC pinned to the lattice. Figure 5 shows the amplitude of $4k_F$ charge correlations divided by system size, i.e., $S_\rho(4k_F)/L$. At fixed $\xi = 10$, we find that this quantity extrapolates to zero in the thermodynamic limit in the LL phase [$K_\rho = 0.383(1)$, $V/t = 3$], and to a finite value in the CDW state ($V/t = 9$). Near the phase boundary, the Kosterlitz-Thouless nature of the transition makes numerical studies difficult and we see that, assuming a linear scaling, $S_\rho(4k_F)/L$ extrapolates to a finite but very small value despite $K_\rho = 0.270(3) > 1/4$. For the unscreened Coulomb potential, $S_\rho(4k_F)/L$ increases logarithmically with system size, and there is no long-range order.[10]

C. Dynamical charge and spin correlations

We now discuss the dynamical spin and charge correlation functions, defined in Eq. (4), as obtained from QMC simulations. We begin with a rather weak interaction $V/t = 1$ and a large screening length $\xi = 10$. CTQMC results for these parameters which, according to Fig. 2, fall into the Hubbard regime, are presented in Fig. 6. Despite the long-range interaction, the spectra closely resemble previous results for the Hubbard model (see, e.g., Ref. 40). In particular, the particle-hole continuum is clearly visible in both the charge and the spin channels. As a result of interactions, the velocities of long-wavelength charge and spin excitations differ by about a factor of 2.

To investigate larger values of V/t, we use the SSE representation. The latter can also be used for the parameters of Fig. 5, but we chose the CTQMC method to demonstrate its applicability to models with long-range interactions. Taking $V/t = 6$, we can explore the whole metallic regime of the model (1) by varying the screening length ξ. Results are shown in Fig. 7.

We first discuss the charge sector. For $\xi = 0.1$, corresponding to the strong-coupling regime of the Hubbard model [$U = 2V(0) = 12t$], the results in Fig. 7(a) look qualitatively similar to Fig. 6(a). However, the distribution of spectral weight over the particle-hole continuum is much more inhomogeneous, with pronounced excitation features along the edges. The charge velocity v_ρ is only slightly smaller than in Fig. 6(a). Upon increasing ξ, we observe a substantial increase of v_ρ, as indicated by the dashed lines; between $\xi = 0.1$ and 1, v_ρ increases from $1.97(2)t$ to $2.64(2)t$. A small charge gap of order $0.1t$, which extrapolates to zero for $L \to \infty$ in the LL phase, is visible in Fig. 7(c), but we can estimate the velocity as $v_\rho > 3.5t$. The increase of v_ρ reflects the fact that the extended interaction promotes $4k_F$ charge order, and thereby increases the stiffness of the charges with respect to long-wavelength excitations. This gap is a finite-size effect caused by the close proximity of the CDW transition. The onset of $4k_F$ fluctuations is also reflected in an incomplete but well visible softening of the excitations at $q = 4k_F$. We will see below that this feature develops into a Bragg peak in the CDW state. A plasmon excitation, one of the hallmark features of the $1/r$ Coulomb potential, is not expected for finite values of ξ, and would in general be very difficult to distinguish from a linear mode in numerical simulations.

In contrast to the charge sector, the effect of ξ on the spin dynamics is very small. In accordance with LL theory, the velocity v_σ of long-wavelength spin excitations remains virtually unchanged upon increasing ξ from 0.1 to 10 [Figs. 7(d) and 7(f)]. However, v_σ is strongly renormalized

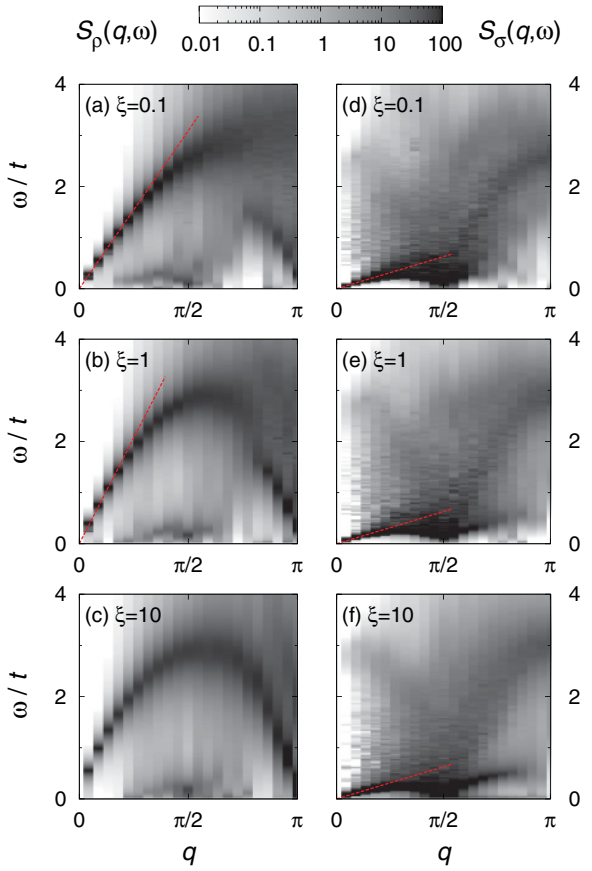

FIG. 7. (Color online) Dynamical charge [(a)–(c)] and spin [(d)–(f)] structure factor from simulations in the SSE representation for $V/t = 6$ and different screening lengths ξ. Results are for $n = 0.5$, $L = 44$, and $\beta t = 2L$. The dashed lines indicate the velocity at long wavelengths.

in going from $V/t = 1$ [Fig. 6(b)] to $V/t = 6$ [Fig. 7(d)]. At fixed V/t, the screening length hence provides a natural way of changing the ratio of charge and spin energy scales, and opens a route to explore the spin-incoherent LL.[41]

Figure 8 shows results for the charge and spin dynamics in the CDW phase, for $V/t = 9$ and $\xi = 10$. As demonstrated in

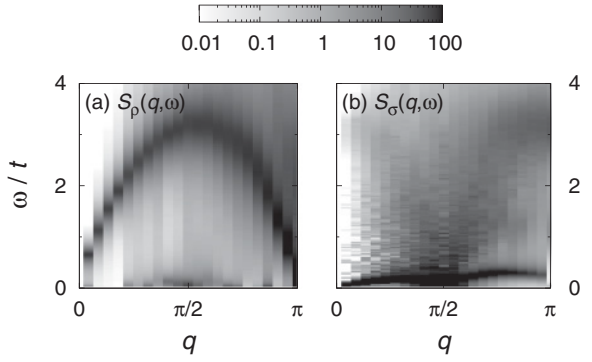

FIG. 8. (a) Dynamical charge and (b) spin structure factor for $V/t = 9$ and $\xi = 10$, corresponding to the insulating CDW phase. Results were obtained in the SSE representation using $n = 0.5$, $L = 44$, and $\beta t = 2L$.

Fig. 5, for these parameters, the system is in a CDW state with long-range $4k_F$ order. In addition to a charge gap at $q = 0$, the charge structure factor has become almost perfectly symmetric with respect to $q = \pi/2$. This doubling of the unit cell results from the softening at $q = 4k_F$, and is a typical signature of the CDW state. Except for a smaller velocity v_σ, the spin structure factor in Fig. 8 is similar to the metallic regime (i.e., gapless) [see for example Fig. 7(c)].

D. Single-particle spectral function

The single-particle spectrum is of particular interest in the search for experimental realizations of LLs because it can reveal the signatures of spin-charge separation (spinon and holon bands).[42,43] Although LL theory is a low-energy description, spin-charge separation may be observed up to rather high energies. For example, spinon and holon bands are visible over an energy range of the order of the bandwidth in the Hubbard model,[40,44,45] and also experimentally for TTF-TCNQ (Ref. 46) and 1D cuprates.[47,48] In contrast, such clear features of spin-charge separation seem to be absent in recent measurements on self-organized gold chains, although the density of states reveals the scaling expected for a LL.[5,49]

To understand the role of the interaction range and small values of K_ρ, we calculate the single-particle spectral function $A(k,\omega-\mu)$ [Eq. (6)] for different values of V and ξ. To simplify the interpretation of the complex structures, we use exact diagonalization on chains with $L = 20$ sites, and use a different graphical representation.

Figure 9 shows the single-particle spectrum in the Hubbard regime for $V/t = 1$ and $\xi = 10$. To highlight the spinon, holon, and shadow bands previously observed for the Hubbard model away from half filling,[40,44,45] we include the holon and shadow band dispersions for the $U = \infty$ Hubbard model,[45] $-2t\cos(|k| + k_F)$ and $-2t\cos(|k| - k_F)$, as well as a linear spinon branch $v_\sigma(k - k_F)$ with v_σ determined from $S_\sigma(q,\omega)$. These analytical results have well-defined corresponding excitations in the numerical spectra, and establish the signatures of spin-charge separation in the Hubbard regime of the phase diagram. The spectral weight of the shadow band at large k is rather small in Fig. 9. The finite spectral weight between the

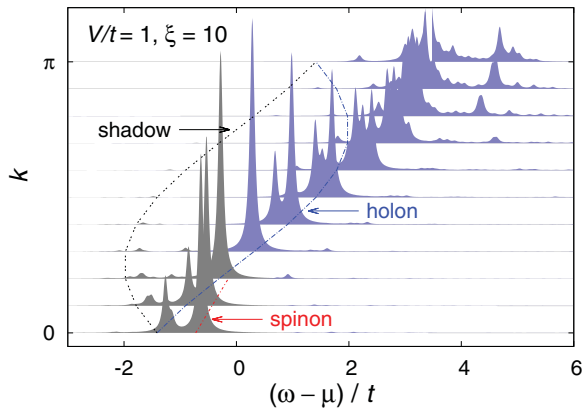

FIG. 9. (Color online) Single-particle spectral function $A(k,\omega-\mu)$ for $n = 0.5$, $V/t = 1$, and $\xi = 10$ from exact diagonalization with $L = 20$. We used an artificial broadening of $0.05t$. The curves marked spinon, holon, and shadow are explained in the text.

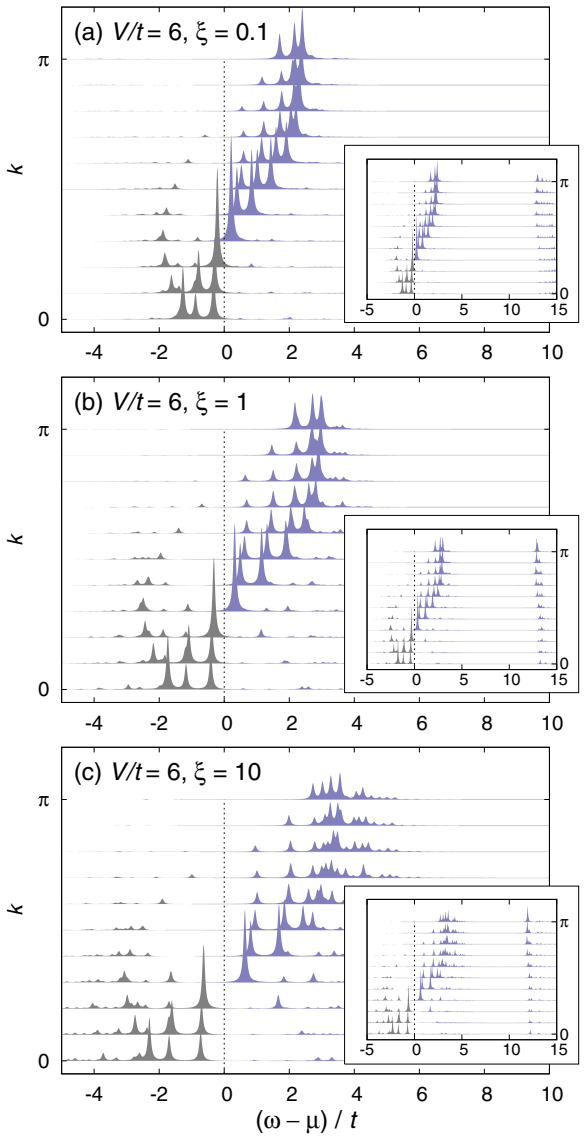

FIG. 10. (Color online) Single-particle spectral function $A(k,\omega-\mu)$ for $n=0.5$, $V/t=6$, and different screening lengths ξ from exact diagonalization with $L=20$. Insets: full energy range, revealing the upper Hubbard band.

holon and spinon excitation peaks is due to the finite system size.[45]

Taking $V/t=6$, we can study the spectral function across the Hubbard, non-Hubbard, and dominant $4k_F$ regimes with increasing ξ. The results are shown in Fig. 10, and reveal that the signatures of spin-charge separation are fully preserved. Whereas the holon dispersion reflects the noticeable increase of the charge velocity with increasing ξ (see Fig. 7), the spinon excitations remain virtually unchanged by the interaction range, again in accordance with the results for $S_\sigma(q,\omega)$ in Fig. 7. The spectral weight of the shadow band is significantly enhanced compared to $V/t=1$ (Fig. 9). On approaching the strong-coupling region at larger ξ, the upper Hubbard band (visible in the insets of Fig. 10) becomes almost completely flat. Similar to Fig. 10, a gap is visible at k_F in Fig. 10(c) [and also in (b) but much smaller]; we have verified that this gap is a finite-size effect.

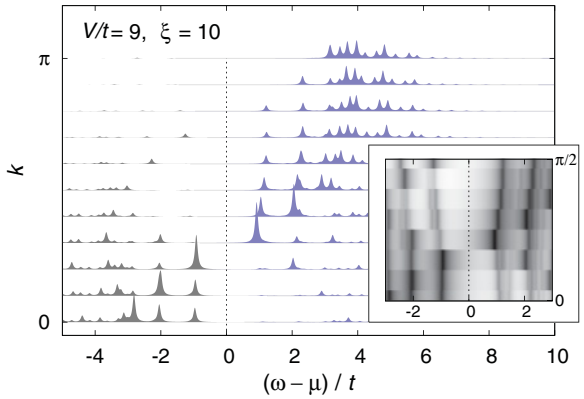

FIG. 11. (Color online) As in Fig. 9 but for $V/t=9$ and $\xi=10$, corresponding to the insulating CDW phase (see Fig. 2). The inset shows a logarithmic density plot of the spectrum, revealing backfolded shadow bands related to the $4k_F$ charge order.

Our findings in the metallic region of the phase diagram are consistent with the experimentally observed coexistence of a small K_ρ (implying extended-range interactions) with signatures of spin-charge separation in photoemission measurements; a good example is TTF-TCNQ.[46] On the other hand, the finite interaction range does not provide an explanation for the possible absence of clear spin-charge separation in self-organized gold chains.[5,49] We comment on the latter case in the conclusions.

Finally, we show in Fig. 11 the single-particle spectrum in the insulating CDW phase at $V/t=9$ and $\xi=10$. The dynamical charge and spin structure factors for these parameters were presented in Fig. 8. We find a charge gap [equal to 0.2(1) in the thermodynamic limit], and backfolded shadow bands related to the $4k_F$ charge order which are visible in the inset of Fig. 11. The spectrum appears to evolve continuously across the CDW transition. In particular, the holon band is well visible in Fig. 11, whereas it has been found to separate into two domain walls for much stronger Coulomb interaction.[22] The single-particle spectrum of a quarter-filled CDW state has also been calculated using the bosonization method.[50] In the absence of dimerization, no singularities exist near k_F (note that in our numerical calculations, we can not distinguish between singularities and excitation peaks of finite width). The spectrum may also depend on the details of the interaction potential.

V. CONCLUSIONS

In this work, we have studied the effects of the electron-electron interaction range in one dimension using exact numerical methods. We have obtained the Luttinger liquid interaction parameter K_ρ as a function of the Coulomb matrix element V and the screening length ξ, which, in combination with Luttinger liquid theory, defines the phase diagram of the model. In addition to the Hubbard regime $1\geqslant K_\rho\geqslant 1/2$, we have explored the non-Hubbard regime $K_\rho<1/2$, the case $K_\rho<1/3$ with dominant $4k_F$ charge correlations, and the insulating CDW state, which exists at quarter filling for $K_\rho<1/4$. We identified an important length scale $1/k_F$ for

K_ρ; K_ρ strongly depends on the screening length for $\xi \lesssim 1/k_F$, whereas it decays very slowly for $\xi \gg 1/k_F$. Our results indicate that the lattice model with a finite (but possibly large) interaction range can be described by Luttinger liquid theory if higher-order umklapp terms are taken into account. This case is therefore distinct from the unscreened $1/r$ potential which falls outside the Luttinger liquid description.[11,12] For the unscreened potential, numerical results suggest the existence of a metallic quasi-Wigner-crystal state with $K_\rho = 0$.[10] For our choice of a screened Coulomb potential, which is both convex and monotonically decreasing with increasing distance, K_ρ always decreases with increasing interaction strength or range, as compared to enhanced metallic behavior observed in extended Hubbard models as a result of competing nearest-neighbor and next-nearest neighbor interactions. Interestingly, the small values of $K_\rho \approx 1/4$ observed in recent experiments on gold chains, as well as previously in quantum wires, carbon nanotubes, and quasi-1D materials, can only be achieved for large values of the interaction strength and/or range.

We have calculated the static and dynamical charge and spin correlation functions, and found good agreement with the expectations based on Luttinger liquid theory. Upon decreasing K_ρ by increasing V and/or ξ, $4k_F$ charge correlations become strongly enhanced, reminiscent of although not identical to the quasi-Wigner-crystal. Our results for the real-space density-density correlations are consistent with Luttinger liquid behavior on length scales beyond the screening length and deviations on smaller length scales.

The $4k_F$ correlations lead to a pronounced Bragg peak in the dynamical density structure factor. The interaction range strongly modifies the velocity of long-wavelength charge excitations, whereas the spin velocity only depends on the onsite repulsion. Throughout the Luttinger liquid phase, spin-charge separation is clearly visible in the single-particle spectrum. Finally, in the insulating charge-density-wave phase, we observe backfolded shadow bands.

An important question to be addressed in future work, motivated by experiments on self-organized gold chains,[5,49] is the impact of spin incoherence on the spinon and holon signatures in photoemission spectra. The energy scales for low-energy charge and spin excitations are determined by the corresponding velocities v_ρ and v_σ. As explicitly shown in this work, v_ρ increases with increasing ξ, whereas v_σ does not depend on the interaction range. Therefore, the charge and spin energy scales can be well separated for sufficiently large ξ. In the regime $v_\rho \gg v_\sigma$, the $2k_F$ spin correlations can be suppressed at finite temperatures, whereas the charge sector remains coherent.[41] This scenario may explain the rather incoherent angle-resolved spectrum of gold chains, which at the same time show clean LL power-law behavior in the angle-integrated density of states.[5]

ACKNOWLEDGMENTS

We thank D. Baeriswyl, R. Claessen, S. Eggert, S. Ejima, F. Essler, H. Fehske, V. Meden, J. Schäfer, and D. Schuricht for helpful discussions. This work was supported by the DFG Grants No. FOR1162 and No. WE 3639/2-1, as well as by the Emmy Noether Programme. We are grateful to the LRZ Munich and the Jülich Supercomputing Centre for generous computer time.

APPENDIX: CTQMC

The general formulation of the weak-coupling CTQMC method allows the simulation of problems with long-range interactions in imaginary time and/or space.[33,34,51] Retarded interactions (i.e., nonlocal in time), which essentially correspond to the electron-phonon problem, have been considered in Refs. 52–54. In this appendix, we provide technical details for the application of the CTQMC method to a Hamiltonian of the form (1).

Although such simulations are in principle straightforward, we have encountered difficulties which are ultimately related to the strong-coupling character of the problem considered in this paper. The algorithm is quite similar to the case of electron-phonon interactions, and has been implemented both at finite temperatures and at $T = 0$ (with a projection parameter θ).[34]

Our starting point is Eq. (1), which we write as

$$H = \sum_k \epsilon(k)\hat{n}_k + \overline{V} \sum_{ir} P(r)\,(\hat{n}_i - n)\,(\hat{n}_{i+r} - n)\,. \quad \text{(A1)}$$

Here, n is the average density, the interaction accounts for fluctuations around the paramagnetic saddle point, and $P(r)$ is a probability distribution; we also defined $\overline{V} = \sum_r V(r)$. During the simulation, vertices corresponding to interactions over a distance r are proposed with probability $P(r) = V(r)/\overline{V}$.

To circumvent the negative sign problem, and following Ref. 34, we rewrite the interaction as

$$\tfrac{1}{2}\overline{V} \sum_{ir\sigma\sigma' s} P(r) \left(\hat{n}_{i\sigma} - \frac{n}{2} + s\delta\right)\left(\hat{n}_{i+r\sigma'} - \frac{n}{2} - s\delta\right). \quad \text{(A2)}$$

Here, we have introduced an Ising variable $s = \pm 1$. Up to a constant, Eq. (A2) is equivalent to the original interaction. To avoid the sign problem for $\overline{V} > 0$ we have the condition $n/2 + \delta > 1$.

The average expansion order, which determines the computer time, can be evaluated within the finite-temperature approach, giving

$$\langle M \rangle = \beta \overline{V} L \left[4\delta^2 - \sum_r P(r) \langle (\hat{n}_0 - n)\,(\hat{n}_r - n)\rangle\right]. \quad \text{(A3)}$$

The fact that the form (A2) is beneficial for the simulations at quarter filling and for rather strong interactions confirms an empirically derived rule. In order to obtain optimal results away from half filling, it is often useful to increase the value of δ at the expense of a larger average expansion order. With the above formulation, we were able to extend the parameter regime of applicability for the weak-coupling CTQMC method, and exemplary results are shown in Fig. 6. However, the strong-coupling regime remains out of reach.

[1] J. Hubbard, Proc. R. Soc. London **276**, 238 (1963).
[2] T. Giamarchi, *Quantum Physics in One Dimension* (Oxford University Press, Oxford, UK, 2004).
[3] J. S. Meyer and K. A. Matveev, J. Phys.: Condens. Matter **21**, 023203 (2009).
[4] V. V. Deshpande and M. Bockrath, Nat. Phys. **4**, 314 (2008).
[5] C. Blumenstein, J. Schäfer, S. Mietke, S. Meyer, A. Dollinger, M. Lochner, X. Y. Cui, L. Patthey, R. Matzdorf, and R. Claessen, Nat. Phys. **7**, 776 (2011).
[6] F. D. M. Haldane, J. Phys. C: Solid State Phys. **14**, 2585 (1981).
[7] V. J. Emery, in *Highly Conducting One-Dimensional Solids*, edited by J. T. Devreese, R. P. Evrard, and V. E. van Doren (Plenum, New York, 1979), Chap. 6, p. 247.
[8] J. Voit, Rep. Prog. Phys. **58**, 977 (1995).
[9] S. Capponi, D. Poilblanc, and T. Giamarchi, Phys. Rev. B **61**, 13410 (2000).
[10] G. Fano, F. Ortolani, A. Parola, and L. Ziosi, Phys. Rev. B **60**, 15654 (1999).
[11] L. I. Glazman, I. M. Ruzin, and B. I. Shklovskii, Phys. Rev. B **45**, 8454 (1992).
[12] H. J. Schulz, Phys. Rev. Lett. **71**, 1864 (1993).
[13] H. Gutfreund and M. Schick, Phys. Rev. **168**, 418 (1968).
[14] J. Hubbard, Phys. Rev. B **17**, 494 (1978).
[15] R. A. Klemm and A. I. Larkin, Phys. Rev. B **19**, 6119 (1979).
[16] M. Fabrizio, A. O. Gogolin, and S. Scheidl, Phys. Rev. Lett. **72**, 2235 (1994).
[17] M. Franco and L. Brey, Phys. Rev. Lett. **77**, 1358 (1996).
[18] A. Iucci and C. Naón, Phys. Rev. B **61**, 15530 (2000).
[19] S. Bellucci and J. Gonzalez, Eur. Phys. J. B **18**, 3 (2000).
[20] D. W. Wang, A. J. Millis, and S. Das Sarma, Phys. Rev. B **64**, 193307 (2001).
[21] B. Valenzuela, S. Fratini, and D. Baeriswyl, Phys. Rev. B **68**, 045112 (2003).
[22] M. Daghofer and P. Horsch, Phys. Rev. B **75**, 125116 (2007).
[23] M. Daghofer, R. M. Noack, and P. Horsch, Phys. Rev. B **78**, 205115 (2008).
[24] V. Barsan, J. Phys.: Condens. Matter **1**, 7961 (1989).
[25] D. Poilblanc, S. Yunoki, S. Maekawa, and E. Dagotto, Phys. Rev. B **56**, R1645 (1997).
[26] P. Schmitteckert and R. Werner, Phys. Rev. B **69**, 195115 (2004).
[27] L. Shulenburger, M. Casula, G. Senatore, and R. M. Martin, Phys. Rev. B **78**, 165303 (2008).
[28] G. E. Astrakharchik and M. D. Girardeau, Phys. Rev. B **83**, 153303 (2011).
[29] R. M. Lee and N. D. Drummond, Phys. Rev. B **83**, 245114 (2011).
[30] S. Ejima, F. Gebhard, S. Nishimoto, and Y. Ohta, Phys. Rev. B **72**, 033101 (2005).
[31] A. W. Sandvik, J. Phys. A: Math. Gen. **25**, 3667 (1992).
[32] O. F. Syljuåsen and A. W. Sandvik, Phys. Rev. E **66**, 046701 (2002).
[33] A. N. Rubtsov, V. V. Savkin, and A. I. Lichtenstein, Phys. Rev. B **72**, 035122 (2005).
[34] F. F. Assaad and T. C. Lang, Phys. Rev. B **76**, 035116 (2007).
[35] K. S. D. Beach, e-print arXiv:cond-mat/0403055.
[36] S. Ejima, F. Gebhard, and S. Nishimoto, Europhys. Lett. **70**, 492 (2005).
[37] H. J. Schulz, Phys. Rev. Lett. **64**, 2831 (1990).
[38] S. A. Söffing, M. Bortz, I. Schneider, A. Struck, M. Fleischhauer, and S. Eggert, Phys. Rev. B **79**, 195114 (2009).
[39] S. Nishimoto and M. Tsuchiizu, Phys. Rev. B **81**, 085116 (2010).
[40] A. Abendschein and F. F. Assaad, Phys. Rev. B **73**, 165119 (2006).
[41] G. A. Fiete, Rev. Mod. Phys. **79**, 801 (2007).
[42] J. Voit, Phys. Rev. B **47**, 6740 (1993).
[43] V. Meden and K. Schönhammer, Phys. Rev. B **46**, 15753 (1992).
[44] K. Penc, K. Hallberg, F. Mila, and H. Shiba, Phys. Rev. Lett. **77**, 1390 (1996).
[45] H. Benthien, F. Gebhard, and E. Jeckelmann, Phys. Rev. Lett. **92**, 256401 (2004).
[46] R. Claessen, M. Sing, U. Schwingenschlogl, P. Blaha, M. Dressel, and C. S. Jacobsen, Phys. Rev. Lett. **88**, 096402 (2002).
[47] B. J. Kim *et al.*, Nat. Phys. **2**, 397 (2006).
[48] C. Kim, A. Y. Matsuura, Z. X. Shen, N. Motoyama, H. Eisaki, S. Uchida, T. Tohyama, and S. Maekawa, Phys. Rev. Lett. **77**, 4054 (1996).
[49] S. Meyer, J. Schafer, C. Blumenstein, P. Hopfner, A. Bostwick, J. L. McChesney, E. Rotenberg, and R. Claessen, Phys. Rev. B **83**, 121411 (2011).
[50] F. H. L. Essler and A. M. Tsvelik, Phys. Rev. Lett. **88**, 096403 (2002).
[51] E. Gull, A. J. Millis, A. I. Lichtenstein, A. N. Rubtsov, M. Troyer, and P. Werner, Rev. Mod. Phys. **83**, 349 (2011).
[52] F. F. Assaad, Phys. Rev. B **78**, 155124 (2008).
[53] M. Raczkowski, P. Zhang, F. F. Assaad, T. Pruschke, and M. Jarrell, Phys. Rev. B **81**, 054444 (2010).
[54] M. Hohenadler, H. Fehske, and F. F. Assaad, Phys. Rev. B **83**, 115105 (2011).